MOLECULAR AND CELLULAR BIOLOGY, Sept. 2003, p. 6494–6506 Vol. 23, No. 18
0270-7306/03/$08.00+0 DOI: 10.1128/MCB.23.18.6494–6506.2003
Copyright © 2003, American Society for Microbiology. All Rights Reserved.

Phagosomes Fuse with Late Endosomes and/or Lysosomes by Extension of Membrane Protrusions along Microtubules: Role of Rab7 and RILP

Rene E. Harrison,[1] Cecilia Bucci,[2] Otilia V. Vieira,[1] Trina A. Schroer,[3] and Sergio Grinstein[1]*

Division of Cell Biology, The Hospital for Sick Children, Toronto, Ontario, Canada M5G 1X8[1]; Dipartimento di Scienze e Tecnologie Biologiche ed Ambientali, Universita degli Studi di Lecce, Lecce, Italy 73100[2]; and Department of Biology, The Johns Hopkins University, Baltimore, Maryland 21218[3]

Received 19 February 2003/Returned for modification 8 May 2003/Accepted 25 June 2003

Nascent phagosomes must undergo a series of fusion and fission reactions to acquire the microbicidal properties required for the innate immune response. Here we demonstrate that this maturation process involves the GTPase Rab7. Rab7 recruitment to phagosomes was found to precede and to be essential for their fusion with late endosomes and/or lysosomes. Active Rab7 on the phagosomal membrane associates with the effector protein RILP (Rab7-interacting lysosomal protein), which in turn bridges phagosomes with dynein-dynactin, a microtubule-associated motor complex. The motors not only displace phagosomes in the centripetal direction but, strikingly, promote the extension of phagosomal tubules toward late endocytic compartments. Fusion of tubules with these organelles was documented by fluorescence and electron microscopy. Tubule extension and fusion with late endosomes and/or lysosomes were prevented by expression of a truncated form of RILP lacking the dynein-dynactin-recruiting domain. We conclude that full maturation of phagosomes requires the retrograde emission of tubular extensions, which are generated by activation of Rab7, recruitment of RILP, and consequent association of phagosomes with microtubule-associated motors.

Leukocytes eliminate pathogens and apoptotic cells by initially engulfing them into a phagocytic vacuole. The vacuole, which is derived from the plasmalemma, needs to undergo extensive remodeling to acquire microbicidal and lytic capabilities (28). Such remodeling, also known as maturation, involves sequential fusion with various components of the endolysosomal pathway and concomitant fission events that maintain the vacuolar size nearly constant (1, 28).

The molecular machinery underlying maturation, particularly the process of phagolysosome formation, is poorly understood. It is generally thought that phagosomal maturation shares some features with the progression of endosomes to lysosomes, a complex process that is orchestrated by Rab GTPases (33). Accordingly, Rab5 and Rab7 have been detected on the membranes of early and intermediate phagosomes, respectively (12, 13, 23). Moreover, using an in vitro reconstitution system, Funato and colleagues (15) found that inhibition of Rab function by addition of excess Rab-GDP dissociation inhibitor impaired phagosome maturation. Inhibition of Rab5 may be at least partly responsible for this effect, since immunodepletion of this protein precluded the fusion of phagosomes with endosomes (2, 3). The mode of action of Rab5 and the possible role of other Rabs, particularly Rab7, in phagosomal maturation remain obscure.

The objective of the present studies was to analyze the involvement of Rab7 and its only known effector, RILP (Rab7-interacting lysosomal protein), in phagolysosome formation by mammalian macrophages. To this end, we transfected cells of the murine monocyte/macrophage line RAW 264.7 with chimeric constructs of enhanced green fluorescent protein (EGFP) and either normal or mutated forms of Rab7 and RILP, and we monitored their distribution, dynamics, and functional effects.

MATERIALS AND METHODS

Reagents. Dulbecco's modified Eagle medium (DMEM) and fetal bovine serum (FBS) were from Wisent Inc. Sheep red blood cells (RBC) and rabbit anti-sheep RBC immunoglobulin G (IgG) were obtained from ICN Biomedicals. Polystyrene beads (diameter, 0.8 or 3.1 μm) were obtained from Bangs Laboratories. FUGENE-6 was from Roche Diagnostics Corp. Cy5- and Cy3-conjugated donkey anti-human, anti-mouse, and anti-rabbit IgG antibodies were all from Jackson ImmunoResearch Laboratories. Texas Red, Cy5-labeled dextran (molecular weight, 10,000), and LysoTracker Red DND-99 were purchased from Molecular Probes. Monoclonal anti-p50 dynamitin and anti-p150-glued antibodies were obtained from BD Transduction Laboratories. The monoclonal anti-hemagglutinin (anti-HA) antibody was purchased from Babco. Monoclonal anti-α-tubulin (B-512) and anti-γ-tubulin (T6557) antibodies and all other reagents were obtained from Sigma-Aldrich.

Cell culture, transfection, and phagocytosis. RAW 264.7 macrophages were cultured in DMEM with 10% heat-inactivated FBS as described previously (31). Cells on 25-mm glass coverslips were transiently transfected with FUGENE-6 according to the manufacturer's instructions and used within 24 h of transfection. The generation of the plasmids used for expression of RILP, RILP-C33, wild-type and mutant forms of Rab7 (T22N and Q67L), dynamitin, and the CC2 domain of p150-glued has been described in detail elsewhere (6, 7, 21).

To preload macrophage lysosomes, RAW cells were incubated with 50 μg of Texas Red-dextran/ml for 2 h, followed by washing and chasing in marker-free growth medium for an additional 2 h prior to overnight transfection (18). To depolymerize microtubules, cells were treated with 10 μM colchicine for 20 min at 4°C following internalization of opsonized particles for 10 min. Phagosomal maturation was then allowed to proceed for 30 min at 37°C in the presence or absence of the microtubule-depolymerizing agent. Control and lumicolchicine-treated cells were handled similarly. Where specified, cells were treated with 100 nM wortmannin for 40 min in serum-free medium prior to phagocytosis. Cells

* Corresponding author. Mailing address: Programme in Cell Biology, Hospital for Sick Children, 555 University Ave., Toronto, Ontario, Canada M5G 1X8. Phone: (416) 813-5727. Fax: (416) 813-5028. E-mail: sga@sickkids.ca.

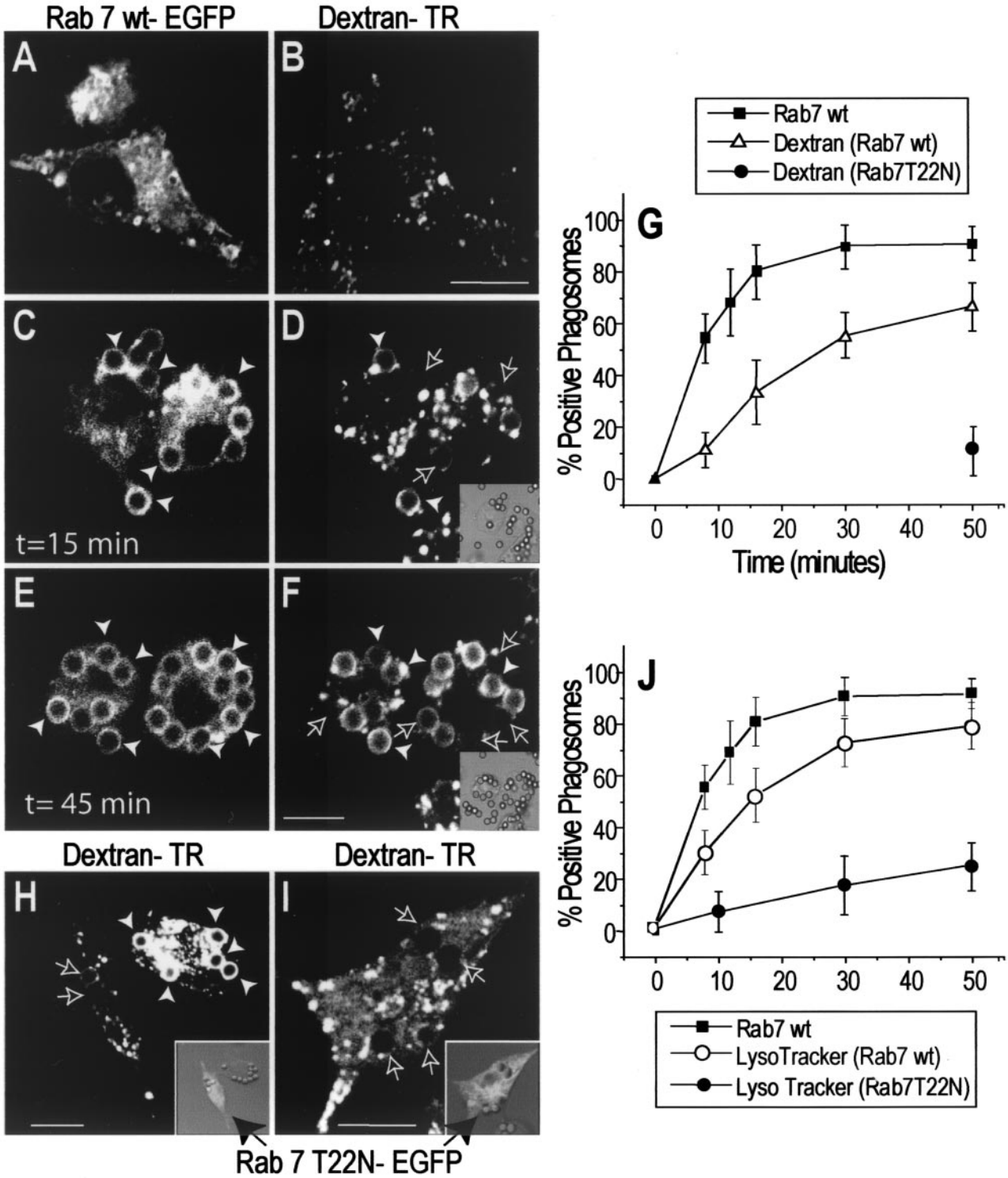

FIG. 1. Role of Rab7 in phagolysosome fusion and acidification. RAW cells were preloaded with Texas Red-dextran as a marker of lysosomes and late endosomes and were transfected with Rab7-EGFP. Phagocytosis was initiated by addition of IgG-opsonized latex beads (time zero), and the reaction was monitored in live cells by confocal fluorescence (main panels) and DIC microscopy (insets). (A through F) Cells were transfected with wild-type Rab7-EGFP, and images were acquired at the times indicated. Green (Rab7) fluorescence (A, C, and E) and the corresponding red (dextran) fluorescence (B, D, and F) are shown. Panels A and B show representative Rab7-EGFP and dextran labeling in a resting cell prior to phagocytosis. White arrowheads point to Rab7- or dextran-labeled phagosomes, while outlined arrows point to unlabeled phagosomes. Adherent, noninternalized beads were identified by staining with a Cy5-conjugated anti-human antibody. (G) The fraction of Rab7wt- or dextran-positive phagosomes was scored, and data for 50 cells from three experiments are summarized. (H and I) Cells transfected with dominant-negative (T22N) Rab7-EGFP were allowed to ingest particles, and images were acquired at 50 min. Insets show an overlay of green fluorescence and DIC images. A longer exposure was used in panel I to confirm the absence of phagosomal labeling. The fraction of dextran-positive phagosomes in Rab7(T22N)-transfected cells was scored and is summarized in panel G. (J) Staining of phagosomes with LysoTracker Red was scored over a 50-min time course. The percentage of Rab7(T22N) phagosomes containing LysoTracker Red is also shown. Data for Rab7(T22N) phagosomes in panels G and J are means ± standard deviations for 30 cells from three experiments. Bars, 10 μm.

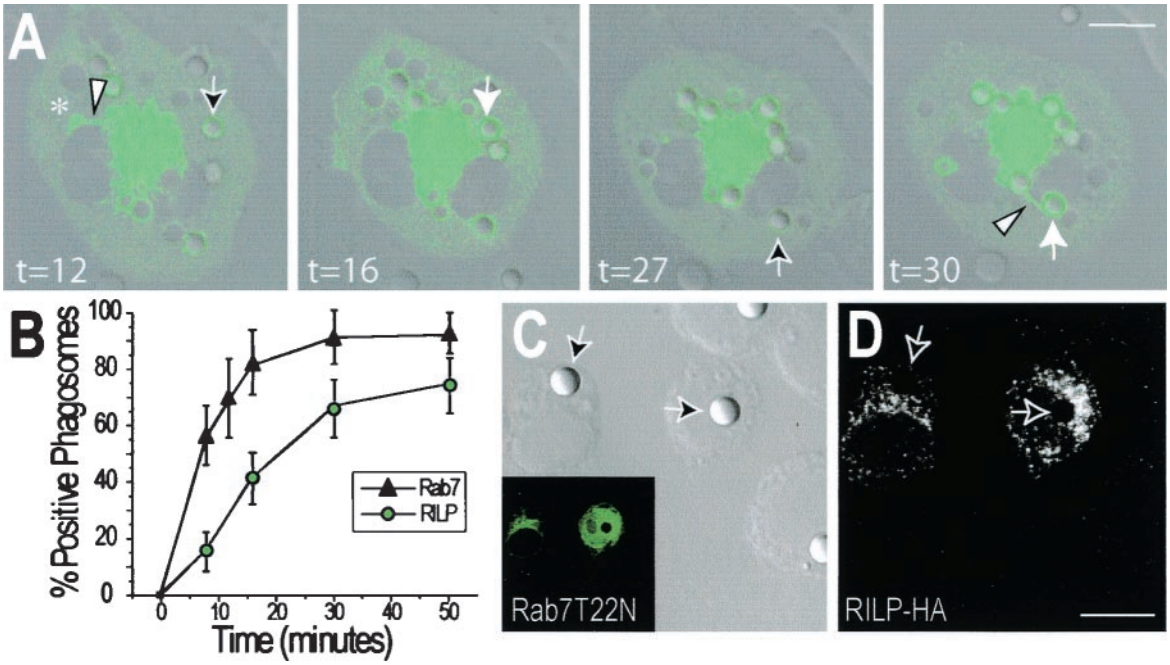

FIG. 2. Phagosomes acquire RILP in a Rab7-GTP-dependent manner. (A) RAW cells were transfected with RILP-EGFP, and after 24 h, phagocytosis was initiated by addition of IgG-opsonized latex beads (time zero). Confocal fluorescence and DIC images were acquired at the indicated times (in minutes) and superimposed. Outlined arrows indicate early phagosomes with little RILP-EGFP, and solid white arrows identify the same phagosomes which had accumulated RILP at a later time. Asterisk denotes a macropinosome. Retrograde tubular extensions often extend from the RILP-positive phagosomes and macropinosomes (arrowheads). (B) Comparison of the time course of acquisition of RILP by phagosomes (from experiments like that for which images are shown in panel A) with that of Rab7 (from Fig. 1). Data are means ± standard deviations for 50 cells from three experiments. (C and D) Cells were cotransfected with Rab7(T22N)-EGFP and epitope-tagged RILP (RILP-HA) and were allowed to internalize particles as in panel A. After 50 min, the cells were fixed and immunostained with anti-HA and Cy3-conjugated secondary antibodies. Arrows point to phagosomes. (C) DIC image (main panel) and corresponding green [Rab7(T22N)-EGFP] fluorescence (inset). (D) Red (RILP-HA) fluorescence. Images in panels A, C, and D are representative of at least 20 cells from three separate experiments. Bars, 10 μm.

were exposed to LysoTracker Red (50 nM) in DMEM for 2 h prior to phagocytosis and imaging.

Sheep RBC and polystyrene beads were opsonized as described elsewhere (31). To induce phagocytosis, RAW cells were exposed to opsonized particles (approximately 5 particles/macrophage) in DMEM-FBS at 37°C for 10 min. Unbound particles were washed off, and cells were incubated for a further 50 min, unless otherwise indicated. To identify opsonized polystyrene beads that were not internalized, the samples were incubated at 4°C with Cy5-labeled donkey anti-human IgG (1:1,000) for 10 min immediately following fixation. Total RBC were stained after permeabilization with a Cy3-conjugated anti-rabbit antibody.

Immunofluorescence and confocal microscopy. Following phagocytosis, RAW cells were washed with phosphate-buffered saline (PBS) and fixed with 4% paraformaldehyde in PBS for 15 min at room temperature. Dextran-containing cells were used immediately for imaging. Immunostaining was performed by permeabilization with 0.1% Triton X-100 in PBS containing 100 mM glycine for 20 min before blocking for 1 h with 5% FBS in PBS. For p50-dynamitin and p-150 glued immunostaining, cells were fixed with methanol (at −20°C) for 10 min, followed by blocking in 5% defatted milk. Staining with primary antibodies was carried out for 1 h at room temperature in PBS containing 1% FBS. Following washing, samples were incubated with appropriate Cy3-conjugated secondary antibodies (1:1,000). For live-cell analysis, coverslips were mounted in a stainless steel chamber and maintained at 37°C with a stage incubator. Images were acquired every 10 or 20 s for periods up to 1.5 h. Samples were analyzed by differential interference contrast (DIC) and fluorescence confocal microscopy using a Zeiss LSM 510 microscope with a 100× oil immersion objective. EGFP, cyan fluorescent protein (CFP), yellow fluorescent protein (YFP), Cy5, and Cy3 were examined by using the conventional laser excitation lines and filter sets. At least 30 cells were quantified for each condition in each experiment. Student's two-tailed *t* tests were performed to assess the significance of differences. Data shown represent means and standard deviations from triplicate experiments.

Electron microscopy. RAW cells were loaded with dialyzed albumin labeled with 10-nm-diameter colloidal gold particles (A_{520}, 1.0) and were chased overnight to ensure lysosomal localization. The cells were then allowed to internalize IgG-opsonized RBC, and after 50 min they were fixed in 2% glutaraldehyde in 0.1 M Sorenson's phosphate buffer, pH 7.2, for 5 min before being scraped off the coverslip and centrifuged. Fixation was continued at room temperature for a further 2 h. Cells were then postfixed in 1% OsO_4 in phosphate buffer at room temperature for 2 h, stained en bloc for 1 h with 1% uranyl acetate in H_2O, and then dehydrated and embedded in Epon resin (EMbed-812; Electron Microscopy Sciences). Sections (thickness, 70 to 80 nm) were collected on copper grids and stained with uranyl acetate and lead citrate. Sections were viewed using a Philips CM 100 electron microscope, and images were captured using a Kodak Megaplus camera, model 1.6i.

RESULTS

Rab7 is required for phagolysosome formation and acidification. The kinetics of association of Rab7 with the phagosome and its relationship to phagolysosome formation were studied using confocal fluorescence microscopy. RAW 264.7 macrophages were transfected with EGFP-tagged Rab7, and their late endocytic organelles (mainly lysosomes) were labeled by preloading with Texas Red-conjugated dextran. An overnight chase period was included in the protocol to ensure that dextran trapped in early endosomes was cleared by recycling and/or delivery to late endosomes and especially lysosomes. Prior to phagocytosis, Rab7 was observed lining dextran-containing vesicles as well as numerous other vesicles likely rep-

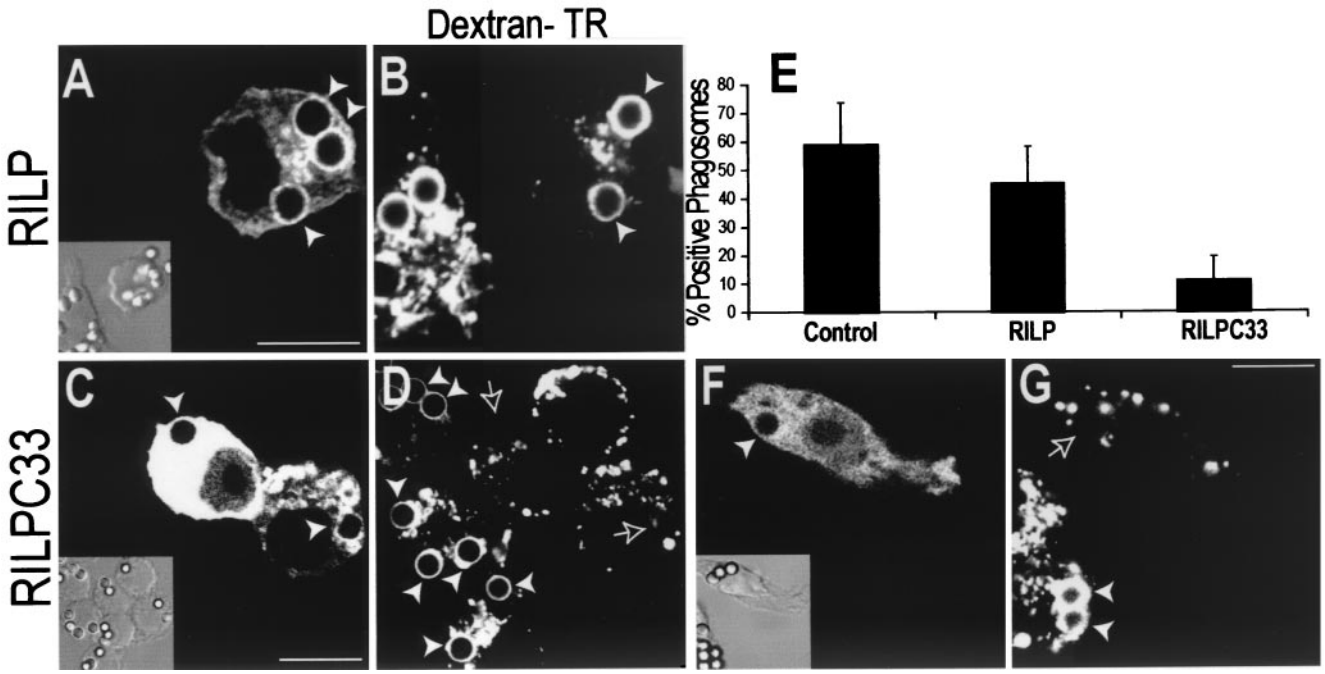

FIG. 3. RILP is necessary for phagolysosome formation. (A to D) RAW cells were preloaded with Texas Red-dextran as a marker of late endosomes and/or lysosomes and were transfected either with wild-type RILP-EGFP (A and B) or with truncated RILP-C33-EGFP (C and D). Phagocytosis of IgG-opsonized latex beads was allowed to proceed for 50 min, and green (A and C) and red (B and D) confocal fluorescence and DIC images (insets) were acquired. (E) The fractions of dextran-positive phagosomes in untransfected cells and in cells transfected with either wild-type or truncated RILP were scored. Data are means ± standard deviations for 30 cells from five experiments. (F and G) RAW cells were preloaded with Cy5-dextran as a marker of late endosomes and/or lysosomes and were cotransfected with cyan-labeled truncated RILP (RILP-C33-CFP) and YFP-labeled, constitutively active Rab7 [Rab7(Q67L)-YFP]. (F) Location of RILP-C33-CFP. (Inset) Corresponding DIC image. (G) Distribution of Cy5-dextran. White arrowheads point to labeled phagosomes, and outlined arrows indicate phagosomes devoid of dextran. Images are representative of at least three experiments of each type. Bars, 10 μm.

resenting earlier compartments of the endocytic pathway, including late endosomes (Fig. 1A and B). Fcγ receptor-mediated phagocytosis was initiated by addition of IgG-opsonized latex beads (time zero). As shown in Fig. 1, Rab7 is acquired by the phagosomal membrane within minutes of particle ingestion; 10 min after initiation of phagocytosis, more than 50% of phagosomes contained Rab7 (Fig. 1C, E, and G). By contrast, significant acquisition of late endosome and lysosomal contents was apparent only after 20 min and reached 50% only after 30 min. Thus, Rab7 acquisition appears to precede fusion of phagosomes with late endosomes and/or lysosomes. Note that Rab7 acquisition precedes the displacement of phagosomes from the periphery toward the center of the cell.

The temporal sequence described above suggests that Rab7 may play a causal role in the formation of phagolysosomes. This notion was tested by transfecting the macrophages with Rab7(T22N), a mutant form of Rab7 with reduced affinity for GTP, which is known to exert a dominant-negative effect. Rab7(T22N) was found largely in the cytosol of RAW cells and never accumulated on the phagosomal membrane (Fig. 1H and I, insets). The phagocytic ability of the cells was unaffected by expression of Rab7(T22N) (data not shown), but we noted that dextran-containing compartments were more peripheral and often smaller in the transfectants, as reported previously (6). More importantly, the dominant-negative mutant greatly depressed the rate of phagolysosome formation (Fig. 1H and I). When measured after 50 min, phagolysosomal fusion reached 62.2% in control cells but was only 10.1% in cells expressing Rab7(T22N) (Fig. 1G). Failure to fuse in dominant-negative transfectants was noted even when longer photographic exposures were used (Fig. 1I) and was therefore understood not to be an artifactual consequence of the lower content of fluid phase marker noted in some cells. We also quantified the effect of Rab7(Q67L), a constitutively active form of Rab7, on the fusion of late endosomes and lysosomes with phagosomes. There was no significant effect of the active Rab7 on the rate of phagolysosome fusion; after 10 min, lysosomal dextran was detectable within phagosomes in 14.1% ± 2.7% of control and 16.3% ± 3.9% of Rab7(Q67L)-transfected cells. Hence, the availability of active Rab7 is not the rate-limiting step in the fusion cascade.

Phagosomes undergo a gradual yet profound acidification during the course of maturation (20). This results from progressive acquisition of vacuolar-type ATPases by fusion of the phagosome with acidic endomembrane compartments. Maximal acidification requires fusion with lysosomes, which are richly endowed with ATPases. We monitored acidification by confocal analysis in live Rab7-transfected cells and determined that acquisition of the GTPase preceded LysoTracker Red accumulation in the phagosome (Fig. 1J). We measured the effect of Rab7(T22N) on phagosomal acidification by using a membrane-permeant acidotropic probe. The accumulation of LysoTracker Red was negligible at early times and was very modest 50 min after particle ingestion (Fig. 1J). Although

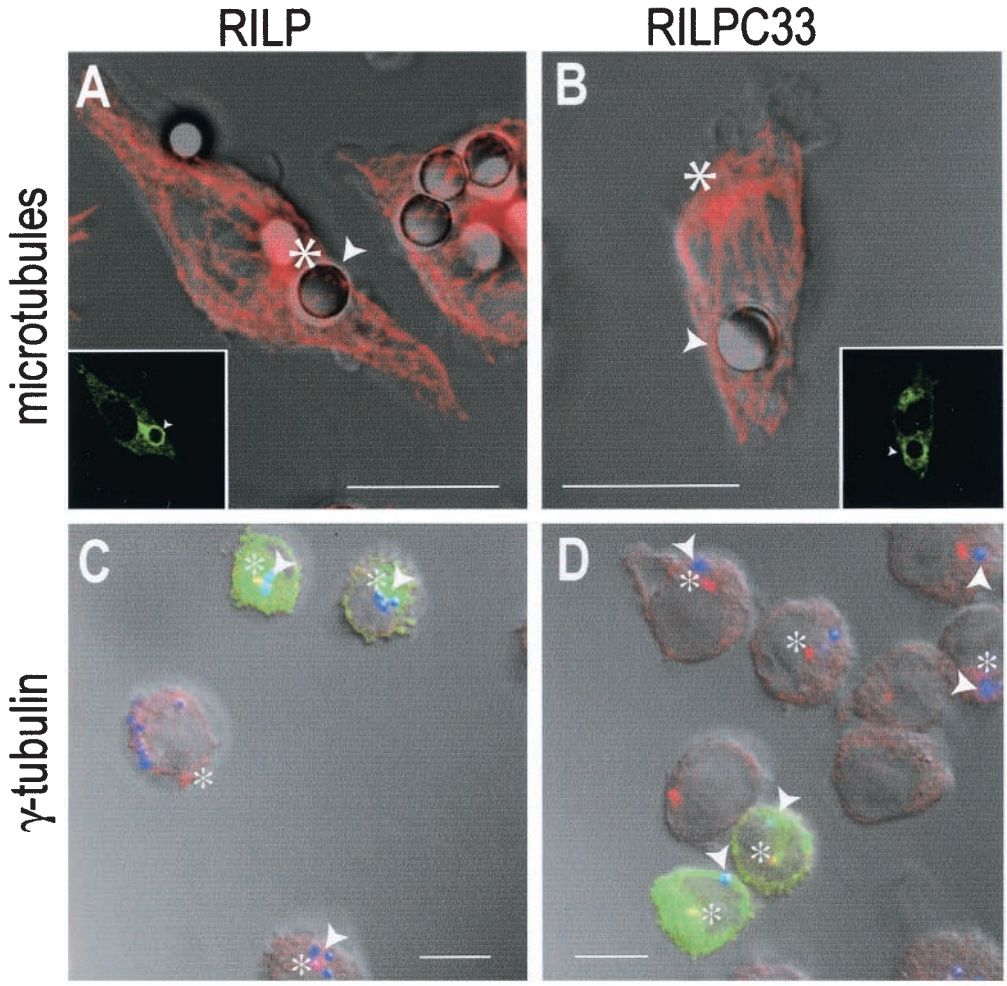

E

Time of phagocytosis (min)	RILP-transfected cells	RILPC33-transfected cells	Control cells
10 min	7.2 ± 0.3	7.0 ± 0.2	7.0 ± 0.3
30 min	3.1 ± 0.2	5.4 ± 0.5	4.2 ± 0.4
50 min	1.5 ± 0.1	4.1 ± 0.2	2.6 ± 0.4

Data are distance of 0.8 μm beads from γ-tubulin immunostained MTOC (in μm)

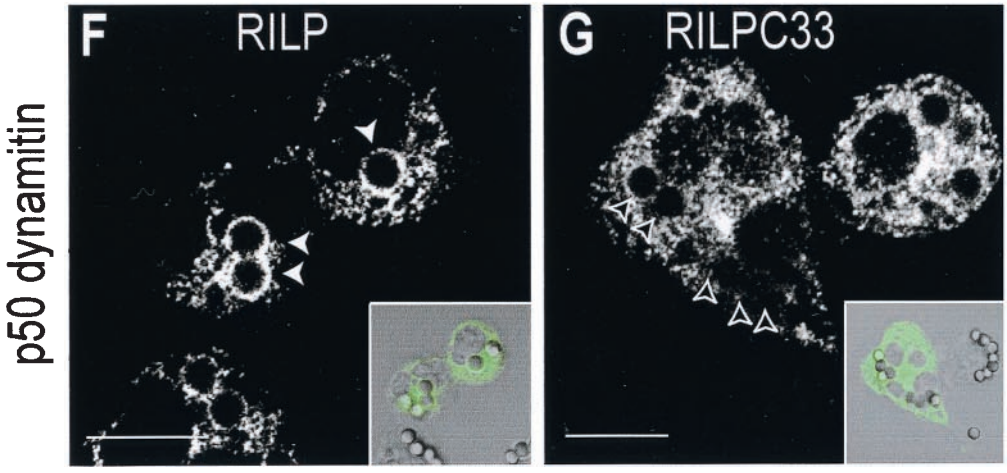

precise determinations of the absolute pH was not undertaken, it is apparent that functional Rab7 is required for optimal phagosomal acidification. Jointly, these experiments indicate that Rab7 is an essential component in the maturation of phagosomes. Our results with mammalian phagocytes differ from those obtained with *Dictyostelium*, where acidification of the phagosome is transient (25). In those cells, impairment of Rab7 did not prevent the initial acidification but accelerated its dissipation (25). Moreover, while acquisition of lysosomal glycosidases was blocked by inhibitory Rab7, cysteine proteases were appropriately delivered to the *Dictyostelium* phagosome. Thus, while Rab7 may play similar roles in mammalian and *Dictyostelium* cells, some differences exist between these systems.

RILP, a Rab7 effector, associates with phagosomes. We proceeded to investigate the mechanism whereby Rab7 may contribute to phagosomal maturation. To our knowledge, only one effector protein of Rab7 has been identified to date, namely, RILP (7, 19). We studied the distribution of RILP in macrophages by transfection of a RILP-EGFP chimeric construct. As reported recently (7, 19), RILP is found on the membranes of late endosomes and/or lysosomes, and its ectopic expression promotes the clustering of these organelles near the microtubule-organizing center (MTOC) (Fig. 2). Shortly after particle ingestion, RILP was also found on the phagosomal membrane (Fig. 2A). As discussed in detail below, RILP-positive phagosomes often extended tubular processes in a retrograde direction (Fig. 2A, $t = 30$). The acquisition of RILP was apparent within minutes of the association of Rab7 with the phagosomes (Fig. 2B). We therefore tested whether Rab7 was required for recruitment of RILP. As shown in Fig. 2C and D, transfection of the cells with Rab7(T22N) precluded association of RILP with the phagosomes. Whereas 73.5% of control phagosomes acquire RILP after 50 min, RILP was never detectable when the dominant-negative Rab7 was coexpressed. Thus, RILP is recruited to phagosomes by active Rab7. We also quantified the effect of constitutively active Rab7 on RILP acquisition, using YFP- and CFP-tagged constructs. After 10 min 22.2% ± 6% and 36.7% ± 4.7% of phagosomes acquired RILP in cells transfected with wild-type Rab7 and Rab7(Q67L), respectively. Clearly, constitutively active Rab7 enhances the phagosomal recruitment of RILP:

RILP is required for phagolysosome formation. We employed a truncated form of RILP, unable to bind to downstream effectors, to assess its possible role in the formation of phagolysosomes. Transfection of wild-type RILP had only a modest effect on phagolysosome fusion (Fig. 3A, B, and E), though a significant inhibition was observed in cells expressing large amounts of the protein (data not shown). As RILP is proposed to stabilize activated Rab7 on late endosomes and lysosomes (7, 19), this effect may be due to depletion of the cytosolic Rab7 pool, reducing its availability for interaction with phagosomes. Truncated RILP (RILP-C33-EGFP) was acquired by phagosomes to an extent that was comparable to that of full-length RILP (data not shown). However, in contrast to the full-length effector, even moderate expression levels of RILP-C33 greatly inhibited the fusion of phagosomes with late endosomes and lysosomes (Fig. 3C to E). After 50 min, only 12.4% of the phagosomes contained a late endosomal or lysosomal marker in cells expressing RILP-C33.

The inhibitory effect of RILP-C33 is exerted downstream of Rab7. This was concluded from experiments where the truncated form of RILP tagged with CFP was expressed jointly with the constitutively active mutant of Rab7 tagged with YFP (Fig. 3F). The inhibition of phagolysosomal fusion persisted under these conditions (Fig. 3G), implying that RILP-C33 was producing inhibition not by preventing the activation of Rab7 but instead by precluding its effector action. These experiments also suggest that the truncated RILP was not acting by scavenging endogenous Rab7 from the cytosolic pool, since overexpression of the active Rab7 failed to overcome the inhibition.

RILP promotes centripetal migration of phagosomes. During the course of maturation, phagosomes migrate from the cell periphery to the vicinity of the MTOC. This centripetal motion was reported to reach speeds of 0.2 to 1.5 μm/s (4), suggestive of microtubule motor-mediated translocation. RILP is likely to participate in this process, considering its ability to interact both with Rab7, a phagosome-associated protein, and (indirectly) with dynein, a microtubule-associated motor. In accordance with this prediction, acquisition of RILP coincided with phagosomal movement towards the perinuclear region, and 50 min after formation, phagosomes decorated with RILP-EGFP were almost always found adjacent to the MTOC (Fig. 4A). By contrast, phagosomes bearing the truncated RILP-C33 were more often found randomly in the cell periphery, away from the MTOC (Fig. 4B). To more quantitatively assess the role of RILP in phagosome migration, we used small latex beads (diameter, 0.8 μm) and precisely located the MTOC by using an antibody to γ-tubulin (Fig. 4C). The distance separating the beads from the MTOC was measured at different time points after phagocytosis, and the data are summarized in Fig. 4E. Expression of exogenous full-length RILP induced a moderate but significant acceleration of the beads towards the MTOC. Conversely, the truncated RILP reduced the rate of centripetal translocation of the beads. The impaired ability to move towards the MTOC is most likely the result of a failure of the phagosomes to recruit the dynein-dynactin complex. As shown in Fig. 4F, one of the components of this complex, p50-dynamitin, is readily observable on the surface of phago-

FIG. 4. RILP promotes dynamitin recruitment and displacement of phagosomes towards the MTOC. RAW cells were transfected with RILP-EGFP (A, C, and F) or RILP-C33-EGFP (B, D, and G) and allowed to internalize 3.1-μm-diameter (A, B, F, and G) or 0.8-μm-diameter (C and D) IgG-coated beads. After 50 min, the cells were fixed, permeabilized, and immunostained for either α-tubulin (A and B), γ-tubulin (C and D), or p50-dynamitin (F and G). Main panels in A and B show α-tubulin staining overlaid on DIC images. Insets show distribution of RILP-EGFP (A) or RILP-C33-EGFP (B). Bars, 10 μm. Panels C and D show smaller beads (blue) overlaid with γ-tubulin (red) and RILP (C) (green) at 30 min and RILP-C33 (D) (green) at 50 min. Asterisks indicate the location of the MTOC. Bars, 5 μm. Quantitation of bead distance from MTOC is shown in panel E. Data are means from four separate experiments. Main panels in F and G show p50-dynamitin staining. Insets show distribution of RILP-EGFP (F) or RILP-C33-EGFP (G) overlaid on DIC images. Arrowheads point to phagosomes. Bars, 10 μm.

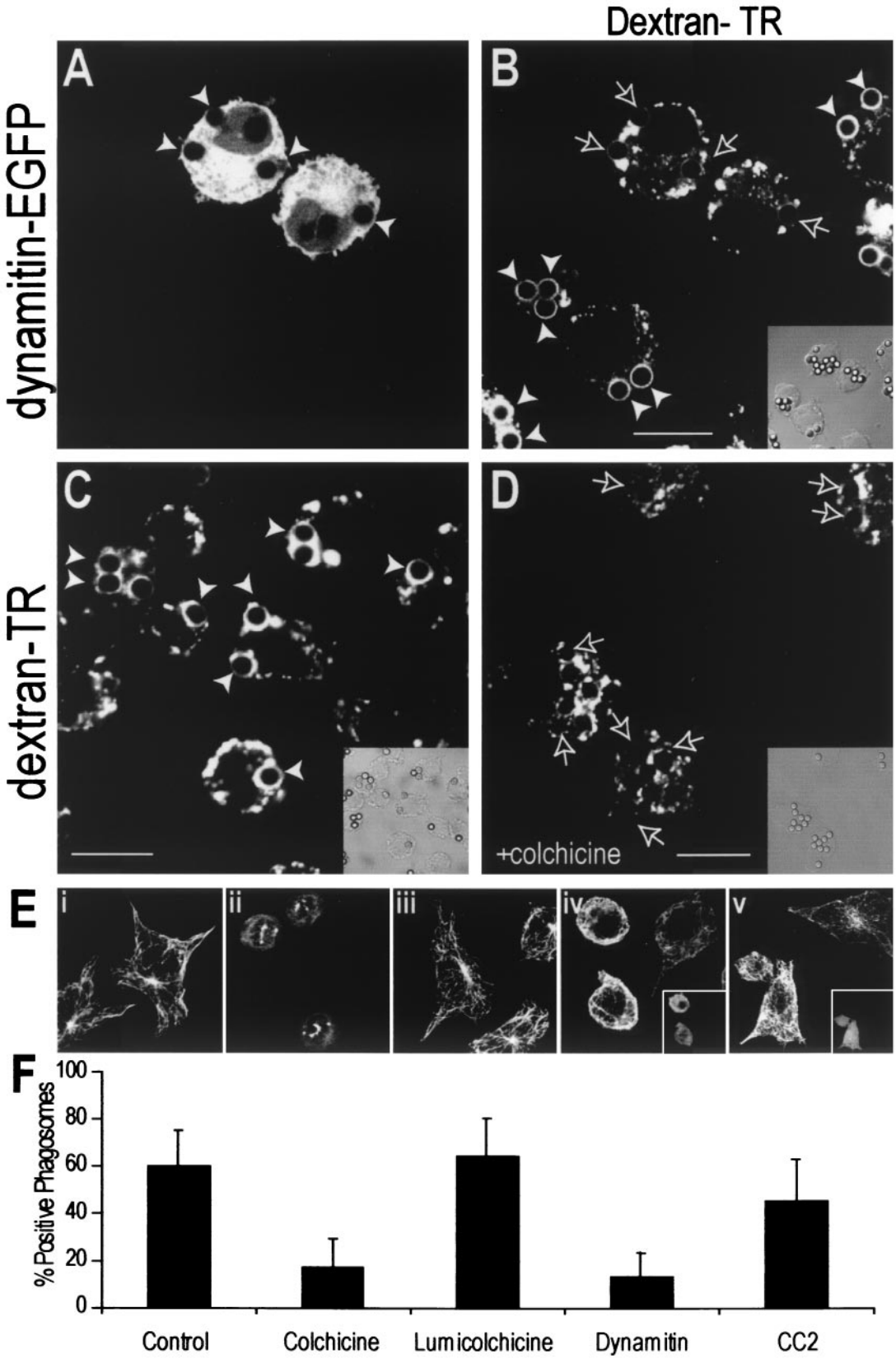
Dextran- TR
A
B
dynamitin-EGFP
C
D
dextran-TR
+colchicine
E
i
ii
iii
iv
v
F
% Positive Phagosomes
100
80
60
40
20
0
Control
Colchicine
Lumicolchicine
Dynamitin
CC2

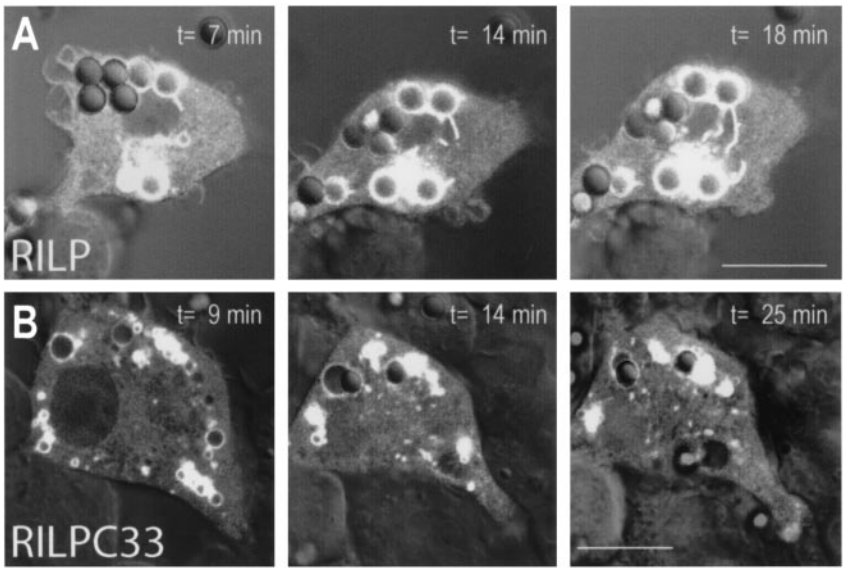

C

Tubule characteristic	RILP-transfected cells
Number of tubules per phagosome	2.1 ± 0.5
Time of tubule appearance after RILP acquisition (min)	6.4 ± 0.5
% Retrograde tubules	71.4 ± 5.0
Maximal length of tubules (μm)	2.8 ± 0.5
Speed of tubule elongation (μm/sec)	0.3 ± 0.1

FIG. 6. Characterization of phagosomal tubules. The fluorescence of RAW cells transfected with RILP-EGFP (A) or RILP-C33-EGFP (B) was monitored by confocal analysis during phagosome maturation. Confocal fluorescence and DIC images were acquired at the indicated times (in minutes) after the appearance of RILP on the phagosomal membrane, and these images were superimposed. The characteristics of the tubules observed in cells transfected with full-length RILP are summarized (C). Means ± standard errors for 20 individual time lapse experiments are presented. The percentage of retrograde tubules was calculated by assuming that the perinuclear late-endosomal–lysosomal cluster observed in RILP-transfected cells reflects the location of the MTOC (see reference 19).

somes transfected with full-length RILP but is not detectable when the cells express RILP-C33 (Fig. 4G). Similar results were obtained using antibodies to p150-glued, another component of the dynactin complex (data not shown).

To verify that the retrograde displacement of phagosomes results from the activity of dynein, we overexpressed p50-dynamitin-EGFP. Overexpression of the wild-type protein has been shown to arrest dynein-mediated organellar motion by uncoupling the motor from its targets (21). Overexpression of dynamitin often displaced both phagosomes and late endocytic compartments towards the periphery of the cells, away from the MTOC (Fig. 5A).

By promoting the apposition of phagosomes and late endosomes and/or lysosomes, Rab7–RILP may favor their interaction and ultimately their fusion. This prediction was also tested by overexpressing dynamitin and measuring the appearance of late-endosome or lysosomal markers in the phagosomal lumen. Uncoupling the dynein-dynactin complex with excess dynamitin significantly inhibited phagolysosome fusion (Fig. 5A, B, and F). This suggests that retrograde migration of phagosomes and/or late endocytic organelles along microtubules facilitates their fusion. This conclusion was confirmed by altering phagosome migration by using colchicine to disrupt the microtubules. As illustrated in Fig. 5C and D and summarized in Fig. 5F, the microtubule-depolymerizing agent clearly reduced the efficiency of phagolysosomal fusion, in agreement with earlier findings (12). Lumicolchicine, a chemical analog of colchicine that lacks the microtubule-depolymerizing effects (Fig. 5E), did not alter phagosome maturation (Fig. 5F). Of note, colchicine did not prevent the association of RILP with the phagosomal membrane, implying that disruption of microtubules did not interfere with signaling events leading to Rab7 recruitment and activation.

Dynamitin overexpression not only uncouples dynein from its cargo but also alters MTOC function and the arrangement of microtubules ((21) (Fig. 5E). To validate the hypothesis that inhibition of phagolysosome formation resulted from the former and not from the latter effect, we compared the effects of dynamitin with those of the CC2 (coiled-coil 2) domain of p150-glued. This CC2 domain similarly alters microtubule ar-

FIG. 5. Microtubule-mediated dynein activity is necessary for phagolysosome formation. (A and B) RAW cells were preloaded with Texas Red-dextran as a marker of late endosomes and/or lysosomes, and dynamitin-EGFP was overexpressed by transfection to disrupt dynein function. Phagocytosis of IgG-opsonized latex beads was allowed to proceed for 50 min, and green (A) and red (B) confocal fluorescence and DIC images (inset) were acquired. (C and D) RAW cells were preloaded with Texas Red-dextran and allowed to internalize beads for 10 min at 37°C. The cells were then either left untreated (C) or cooled and treated with 10 μM colchicine for 20 min before maturation was allowed to proceed for an additional 30 min at 37°C. The dextran distribution is shown in the main panels, and the corresponding DIC is shown in the insets. White arrowheads indicate dextran-positive phagosomes, whereas outlined arrows mark phagosomes without dextran accumulation. Bars, 10 μm. (E) Tubulin immunostaining in control (i), colchicine-treated (ii), lumicolchicine-treated (iii), dynamitin-overexpressing (iv), and CC2 domain-expressing (v) cells. The transfected cells in panels iv and v are shown in the insets. (F) Phagosomal maturation was measured by the acquisition of Texas Red-dextran in either control cells, colchicine- or lumicolchicine-treated cells, or cells expressing dynamitin or the CC2 domain. Data are means ± standard deviations for 30 cells from three experiments.

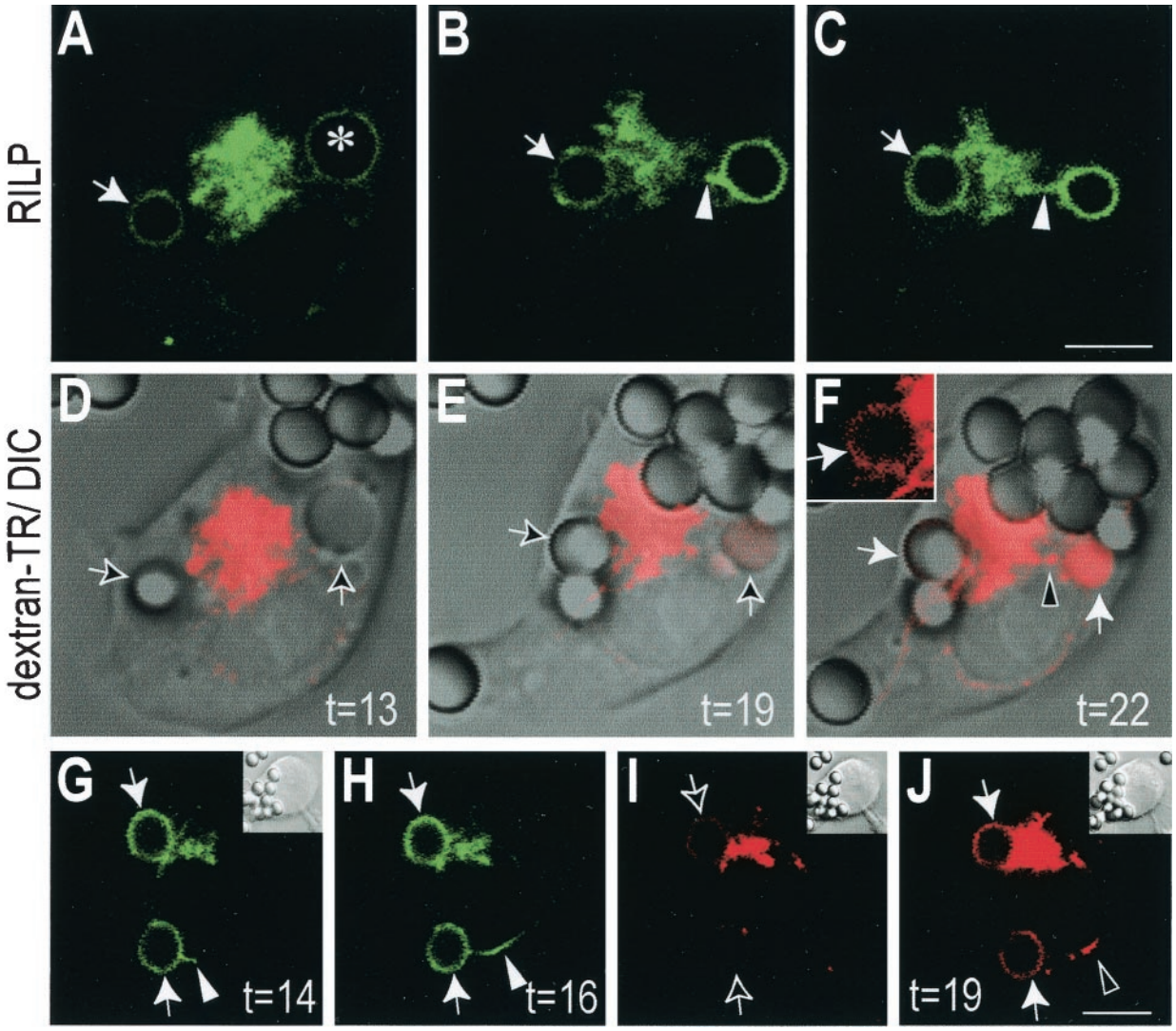

FIG. 7. Fusion of phagosomes with late endosomes and/or lysosomes proceeds via RILP-containing retrograde extensions. RAW cells were preloaded with Texas Red-dextran as a marker of late endosomes and lysosomes and were transfected with RILP-EGFP. At time zero, phagocytosis was initiated by addition of IgG-opsonized beads, and the reaction was monitored by simultaneous fluorescence confocal and DIC microscopy. (A through C) Green (RILP) fluorescence. (D through F) Corresponding red (dextran) fluorescence, overlaid on DIC images. Inset in panel F shows the fluorescence of phagosome indicated by the horizontal white arrow in the main panel. A macropinosome is identified by an asterisk in panel A. The time after addition of beads (in minutes) is indicated. (G through J) An independent experiment. Green (RILP) fluorescence at the times indicated (G and H) and red (dextran) fluorescence corresponding to 16 and 19 min (I and J) are shown. Note the appearance of lysosomal label in the phagosomal lumen between 16 and 19 min. Phagosomes are indicated by arrows, and arrowheads point to tubular extensions. Bars, 5 μm.

chitecture ((21) (Fig. 5E) yet lacks the motor-uncoupling effect that dynamitin exerts on endomembranes. Overexpression of the CC2 domain did not significantly decrease late-endosome or lysosomal fusion with the phagosome (Fig. 5F), suggesting that the effects of dynamitin on phagolysosomal fusion are unrelated to the disruption of microtubule organization.

Phagosomes emit tubular projections that fuse with late endosomes and/or lysosomes. To better understand the mechanism whereby RILP promotes phagolysosomal fusion, we undertook a detailed temporal analysis using fluorescence and DIC microscopy. As intimated earlier, we frequently saw RILP-positive tubules extending from phagosomes towards the MTOC, where late endosomes and/or lysosomes were clustered. A typical example is shown in Fig. 6, where the progressive elongation of RILP-containing tubular structures was monitored over time. Note that the tubular extensions almost always formed in the direction of the MTOC and were rarely centrifugal. The properties of such tubules were quantified in 20 similar time lapse experiments and are summarized in Fig. 6C. Tubules were seen to extend from phagosomes in practically every cell analyzed. The tubules were first apparent ≈6 min after RILP was acquired by the phagosome, and 71% of them were directed towards the MTOC. The speed of tubule elongation averaged 0.3 μm/s. Together with the preferential displacement towards the MTOC, the elongation speed is consistent with mediation by microtubule-associated motors, likely

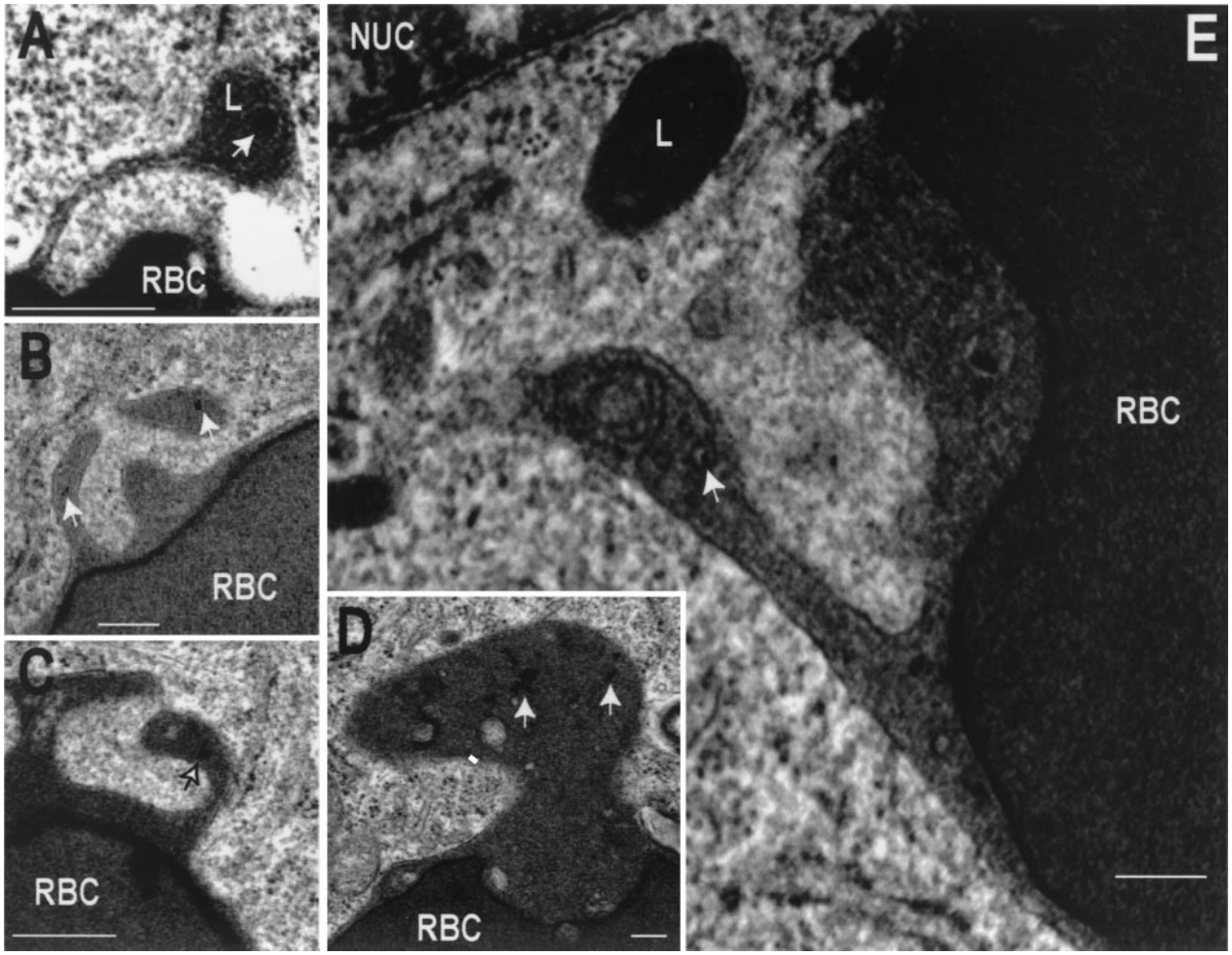

FIG. 8. Transmission electron microscopy of phagosomal tubules. The late-endosomal–lysosomal compartment of RAW cells was labeled by pulsing with colloidal gold-conjugated albumin, followed by an overnight chase. The cells were then allowed to internalize IgG-coated RBC, and after 50 min, they were fixed and processed for transmission electron microscopy. Micrographs show the presence of tubules extending from phagosomes. The tubules are often oriented towards the nucleus (NUC) and in the vicinity of electron-dense lysosomes (L). Some of the tubules contain gold-labeled particles (arrows). In panel E the tubule has seemingly fused with a multivesicular body. Bars, 0.2 μm.

dynein. Accordingly, the number of tubules observed and their maximal length were drastically reduced by treatment of the cells with colchicine (0.4 ± 0.2 per phagosome and 1.3 ± 0.2 μm, respectively). It is noteworthy that the tubules not only contained RILP but required the normal function of the protein for their elongation. In cells transfected with the inhibitory form of RILP, RILP-C33, very few, short tubules were observed (Fig. 6B). On average, only 0.2 ± 0.1 tubule per phagosome was noted, and when present, tubules attained a maximal length of only 1.1 ± 0.2 μm.

To study the possible interaction between the tubules emitted by phagosomes and lysosomes, we preloaded the latter with a red fluorescent lysosomal marker and transfected the cells with RILP-EGFP (Fig. 7). A typical example is shown in Fig. 7A to F, where a macropinosome had been formed along with a phagosome. Following the formation of the RILP-containing protrusions, late-endosome or lysosomal markers became detectable in the lumen of the organelles. This is more clearly apparent in the case of the macropinosome because of its larger aqueous volume (Fig. 7F). However, close inspection of the thin rim of solution lining the bead revealed that fusion had occurred in the case of the phagosome also (Fig. 7F inset). The temporal sequence of events is better defined in Fig. 7G to J, where a longer protrusion was formed that reached around the nucleus towards the lysosomal cluster. Note that at 14 min, only a short tubule had extended (Fig. 7G) and no dextran was detectable in the phagosome. By 16 min, the tubule had extended considerably, yet very little late-endosomal or lysosomal dextran had reached the phagosome. Shortly thereafter, however (t = 19 min), dextran had clearly been delivered to the phagosome, despite the fact that most of the late endosomes and/or lysosomes remained clustered near the MTOC, away from the phagosome. We cannot exclude the possibility that late endosomes or lysosomes may have moved centrifugally, perhaps at a different focal plane, to fuse with the phagosome. However, observation of multiple events of this sort leads us to suggest instead that the phagosomal extension reaches and fuses with late-endocytic organelles near the MTOC, serving as

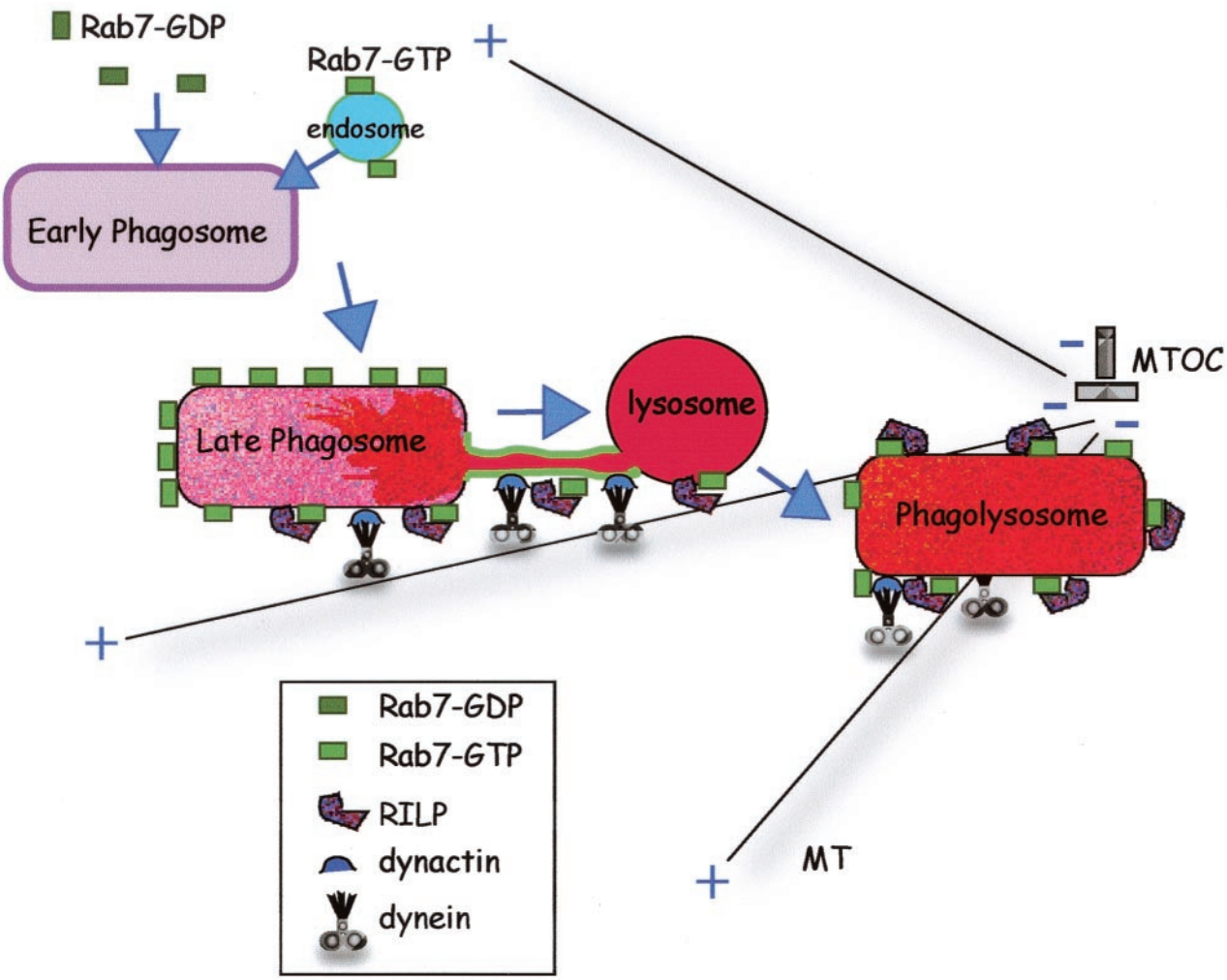

FIG. 9. A model of the role of Rab7–RILP in phagolysosome formation. Following internalization, the early phagosome acquires Rab7 either from a soluble pool and/or by fusion with Rab7-containing endosomes. Rab7-GTP then recruits RILP, which in turn promotes dynein-dynactin association with the phagosome. This complex mediates retrograde movement of phagosomes along microtubules towards the MTOC and in addition promotes the formation of tubular extensions which fuse with late endosomes and lysosomes. Eventually, phagosomes and late endosomes and/or lysosomes merge into a single hybrid organelle.

a conduit for the delivery of late-endosome and lysosomal contents. Moreover, overexpression of inhibitory (headless) kinesin constructs which impair the centrifugal movement of lysosomes did not prevent phagolysosome formation (data not shown).

We also documented the tubulation of phagosomes and their interaction with late endosomes and lysosomes by electron microscopy (Fig. 8). To this end, we preloaded late endosomes and lysosomes with colloidal gold-labeled albumin. Despite the use of normal fixation protocols, known to induce shrinkage and/or fragmentation of tubular structures, we nevertheless were able to observe numerous tubular structures protruding from phagosomes. Gold-labeled particles were often found in such tubules, which occasionally merged with electron-dense structures (Fig. 8E). Of note, these experiments were performed using untransfected RAW cells, implying that ectopic (over)expression of RILP is not required for tubule formation.

DISCUSSION

Centripetal displacement of phagosomes had been documented earlier (12, 29), and the involvement of microtubules and dynein was suggested by in vitro experiments where isolated phagosome motility was reconstituted in a cell-free system (5). However, the machinery linking phagosomes to microtubules had not been identified. Here we show that interaction of phagosomes with dynein requires functional RILP and that the latter is recruited to the phagosomal membrane by active, GTP-bound Rab7.

Several lines of evidence suggest that the Rab7–RILP complex is important not only for phagosomal displacement but also for successful phagolysosomal fusion. Firstly, recruitment of Rab7 by phagosomes was found to precede and to be essential for optimal fusion with lysosomes and other late-endocytic organelles (Fig. 1). Secondly, phagosomal association of RILP, which follows shortly after Rab7 recruitment, was also

essential for fusion with late-endocytic compartments (Fig. 3). Thirdly, tubular extensions were detected to protrude from phagosomes in the direction of the MTOC, where they connected to late endosomes and lysosomes, providing a conduit for delivery of late-endocytic contents to the phagosomal lumen. The proposed centripetal extension of tubules from the phagosome may be related to the ability of late endosomes and/or lysosomes to form a tubular network in macrophages (22). These events are summarized in the diagram presented in Fig. 9. The model differs somewhat from the "kiss-and-run" hypothesis (12), which proposes that luminal contents are delivered to phagosomes by brief, transient interactions with endosomes and lysosomes. We have observed tubules that seemingly remain connected to phagosomes for many seconds after delivery of late-endosomal or lysosomal contents has occurred. Thus, only long, ardent kisses are compatible with the "kiss-and-run" hypothesis. The observation that fusion of phagosomes with late endosomes and lysosomes occurs, at least in part, via thin tubular extensions also seems to differ from the model recently proposed for yeast vacuoles, where large areas of apposition of membranes along a vertex are seemingly required for the fusion event (32). It therefore appears that multiple modes of fusion may exist in different systems.

Dynein has been proposed to exert a fusogenic effect per se, as microtubule motor action causes membrane deformations that may facilitate membrane coalescence (8, 24). However, it would be premature to assign all the fusogenic effects of Rab7 to the motor activity associated with RILP. While RILP is the sole effector of Rab7 described to date, there is precedent for the existence of multiple effectors for other Rab family members (27), and other Rab7-associated proteins are likely to be discovered in the future. In this regard, it is noteworthy that while pretreatment with wortmannin was recently reported to preclude phagolysosome fusion (14, 31), binding of Rab7 and RILP to the phagosomes was only modestly affected (data not shown). This implies that completion of fusion requires additionally one or more events that depend on the activity of class I or III phosphatidylinositol 3-kinase. These may represent other effectors of Rab7 or, alternatively, parallel synergistic pathways, perhaps involving delivery or priming of SNAREs. It is tempting to speculate that the tips of the tubules that extend from phagosomes contain not only Rab7 and RILP but also activated components of the fusogenic machinery.

An unexpected by-product of our experiments was the realization that macropinosomes, which are often formed during the stimulation of phagocytes, also recruit Rab7 and RILP and extend tubules that connect with late endosomes and lysosomes. This observation is of particular significance because certain forms of phagocytosis, such as the engulfment of apoptotic bodies triggered by phosphatidylserine receptors, are thought not to proceed by "zippering," as postulated for Fcγ receptors, but instead to be akin to macropinocytosis (17). Our observations predict that migration along microtubules and fusion with late-endocytic organelles would occur by similar mechanisms in these systems.

Impairment of Rab7 function limited the degree of acidification of the phagosomal lumen. Incomplete acidification is also a well-established feature of phagosomes that contain virulent mycobacteria or *Salmonella enterica* serovar Typhimurium (10, 11), which raises the possibility that similar mechanisms may be involved in both instances. There is an ongoing debate as to whether Rab7 is present in phagosomes containing live mycobacteria (9) or is excluded by a mechanism that arrests maturation at the Rab5 stage (30), and a similar discrepancy exists regarding *Salmonella* (see references 16 and 26). If, as the more recent reports seem to indicate, Rab7 is indeed present in the bacterial phagosomes, association with RILP may be used to assess its state of activation and whether bacterial factors have impaired maturation by preventing the centripetal displacement of the phagosomes or the projection of fusogenic tubules.

ACKNOWLEDGMENTS

We thank Robert Temkin and David Bazett-Jones for help with electron microscopy.

This work was supported by the Canadian Institutes of Health Research (CIHR), the Canadian Arthritis Society, and the National Sanatorium Association. This work was also partially supported by MIUR-PRIN 2001054232 and 2002054531 (to C.B.). R.E.H. is the recipient of a RESTRACOMP Fellowship from the Hospital for Sick Children. O.V.V. is the recipient of a postdoctoral fellowship from PRAXIS XX1 (BPD/22039/99). S.G. is a CIHR Distinguished Scientist and the current holder of the Pitblado Chair in Cell Biology and has been cross-appointed to the Department of Biochemistry, University of Toronto.

R.E.H. and C.B. contributed equally to this work.

REFERENCES

1. **Allen, L. A., and A. Aderem.** 1996. Mechanisms of phagocytosis. Curr. Opin. Immunol. **8:**36–40.
2. **Alvarez-Dominguez, C., A. M. Barbieri, W. Beron, A. Wandinger-Ness, and P. D. Stahl.** 1996. Phagocytosed live *Listeria monocytogenes* influences Rab5-regulated in vitro phagosome-endosome fusion. J. Biol. Chem. **271:**13834–13843.
3. **Alvarez-Dominguez, C., and P. D. Stahl.** 1999. Increased expression of Rab5a correlates directly with accelerated maturation of *Listeria monocytogenes* phagosomes. J. Biol. Chem. **274:**11459–11462.
4. **Blocker, A., G. Griffiths, J. C. Olivo, A. A. Hyman, and F. F. Severin.** 1998. A role for microtubule dynamics in phagosome movement. J. Cell Sci. **111:**303–312.
5. **Blocker, A., F. F. Severin, J. K. Burkhardt, J. B. Bingham, H. Yu, J. C. Olivo, T. A. Schroer, A. A. Hyman, and G. Griffiths.** 1997. Molecular requirements for bi-directional movement of phagosomes along microtubules. J. Cell Biol. **137:**113–129.
6. **Bucci, C., P. Thomsen, P. Nicoziani, J. McCarthy, and B. van Deurs.** 2000. Rab7: a key to lysosome biogenesis. Mol. Biol. Cell **11:**467–480.
7. **Cantalupo, G., P. Alifano, V. Roberti, C. B. Bruni, and C. Bucci.** 2001. Rab-interacting lysosomal protein (RILP): the Rab7 effector required for transport to lysosomes. EMBO J. **20:**683–693.
8. **Chernomordik, L.** 1996. Non-bilayer lipids and biological fusion intermediates. Chem. Phys. Lipids **81:**203–213.
9. **Clemens, D. L., B. Y. Lee, and M. A. Horwitz.** 2000. *Mycobacterium tuberculosis* and *Legionella pneumophila* phagosomes exhibit arrested maturation despite acquisition of Rab7. Infect. Immun. **68:**5154–5166.
10. **Crowle, A. J., R. Dahl, E. Ross, and M. H. May.** 1991. Evidence that vesicles containing living, virulent *Mycobacterium tuberculosis* or *Mycobacterium avium* in cultured human macrophages are not acidic. Infect. Immun. **59:** 1823–1831.
11. **Cuellar-Mata, P., N. Jabado, J. Liu, W. Furuya, B. B. Finlay, P. Gros, and S. Grinstein.** 2002. Nramp1 modifies the fusion of *Salmonella typhimurium*-containing vacuoles with cellular endomembranes in macrophages. J. Biol. Chem. **277:**2258–2265.
12. **Desjardins, M., L. A. Huber, R. G. Parton, and G. Griffiths.** 1994. Biogenesis of phagolysosomes proceeds through a sequential series of interactions with the endocytic apparatus. J. Cell Biol. **124:**677–688.
13. **Duclos, S., R. Diez, J. Garin, B. Papadopoulou, A. Descoteaux, H. Stenmark, and M. Desjardins.** 2000. Rab5 regulates the kiss and run fusion between phagosomes and endosomes and the acquisition of phagosome leishmanicidal properties in RAW 264.7 macrophages. J. Cell Sci. **113:**3531–3541.
14. **Fratti, R. A., J. M. Backer, J. Gruenberg, S. Corvera, and V. Deretic.** 2001. Role of phosphatidylinositol 3-kinase and Rab5 effectors in phagosomal biogenesis and mycobacterial phagosome maturation arrest. J. Cell Biol. **154:**631–644.
15. **Funato, K., W. Beron, C. Z. Yang, A. Mukhopadhyay, and P. D. Stahl.** 1997.

Reconstitution of phagosome-lysosome fusion in streptolysin O-permeabilized cells. J. Biol. Chem. **272:**16147–16151.
16. **Hashim, S., K. Mukherjee, M. Raje, S. K. Basu, and A. Mukhopadhyay.** 2000. Live Salmonella modulate expression of Rab proteins to persist in a specialized compartment and escape transport to lysosomes. J. Biol. Chem. **275:**16281–16288.
17. **Hoffmann, P. R., A. M. deCathelineau, C. A. Ogden, Y. Leverrier, D. L. Bratton, D. L. Daleke, A. J. Ridley, V. A. Fadok, and P. M. Henson.** 2001. Phosphatidylserine (PS) induces PS receptor-mediated macropinocytosis and promotes clearance of apoptotic cells. J. Cell Biol. **155:**649–659.
18. **Hollenbeck, P. J., and J. A. Swanson.** 1990. Radial extension of macrophage tubular lysosomes supported by kinesin. Nature **346:**864–866.
19. **Jordens, I., M. Fernandez-Borja, M. Marsman, S. Dusseljee, L. Janssen, J. Calafat, H. Janssen, R. Wubbolts, and J. Neefjes.** 2001. The Rab7 effector protein RILP controls lysosomal transport by inducing the recruitment of dynein-dynactin motors. Curr. Biol. **11:**1680–1685.
20. **Krause, K. H.** 2000. Professional phagocytes: predators and prey of microorganisms. Schweiz Med. Wochenschr. **130:**97–100.
21. **Quintyne, N. J., S. R. Gill, D. M. Eckley, C. L. Crego, D. A. Compton, and T. A. Schroer.** 1999. Dynactin is required for microtubule anchoring at centrosomes. J. Cell Biol. **147:**321–334.
22. **Racoosin, E. L., and J. A. Swanson.** 1993. Macropinosome maturation and fusion with tubular lysosomes in macrophages. J. Cell Biol. **121:**1011–1020.
23. **Roberts, R. L., M. A. Barbieri, J. Ullrich, and P. D. Stahl.** 2000. Dynamics of rab5 activation in endocytosis and phagocytosis. J. Leukoc. Biol. **68:**627–632.
24. **Roux, A., G. Cappello, J. Cartaud, J. Prost, B. Goud, and P. Bassereau.** 2002. A minimal system allowing tubulation with molecular motors pulling on giant liposomes. Proc. Natl. Acad. Sci. USA **99:**5394–5399.
25. **Rupper, A., B. Grove, and J. Cardelli.** 2001. Rab7 regulates phagosome maturation in *Dictyostelium.* J. Cell Sci. **114:**2449–2460.
26. **Scott, C. C., P. Cuellar-Mata, T. Matsuo, H. W. Davidson, and S. Grinstein.** 2002. Role of 3-phosphoinositides in the maturation of *Salmonella*-containing vacuoles within host cells. J. Biol. Chem. **277:**12770–12776.
27. **Stenmark, H., and V. M. Olkkonen.** 2001. The Rab GTPase family. Genome Biol. **2:**REVIEWS 3007.
28. **Tjelle, T. E., T. Lovdal, and T. Berg.** 2000. Phagosome dynamics and function. Bioessays **22:**255–263.
29. **Toyohara, A., and K. Inaba.** 1989. Transport of phagosomes in mouse peritoneal macrophages. J. Cell Sci. **94:**143–153.
30. **Via, L. E., D. Deretic, R. J. Ulmer, N. S. Hibler, L. A. Huber, and V. Deretic.** 1997. Arrest of mycobacterial phagosome maturation is caused by a block in vesicle fusion between stages controlled by rab5 and rab7. J. Biol. Chem. **272:**13326–13331.
31. **Vieira, O. V., R. J. Botelho, L. Rameh, S. M. Brachmann, T. Matsuo, H. W. Davidson, A. Schreiber, J. M. Backer, L. C. Cantley, and S. Grinstein.** 2001. Distinct roles of class I and class III phosphatidylinositol 3-kinases in phagosome formation and maturation. J. Cell Biol. **155:**19–25.
32. **Wang, L., E. S. Seeley, W. Wickner, and A. J. Merz.** 2002. Vacuole fusion at a ring of vertex docking sites leaves membrane fragments within the organelle. Cell **108:**357–369.
33. **Zerial, M., and H. McBride.** 2001. Rab proteins as membrane organizers. Nat. Rev. Mol. Cell. Biol. **2:**107–117.